AIAA 81-1443R

Afterbody Configuration Effects on Model Forebody and Afterbody Drag

E. R. Thompson* and C. L. Smith†
Arnold Engineering Development Center, Arnold Air Force Station, Tenn.

An experimental investigation was conducted to obtain additional information necessary to complete a study of the influence of changes in afterbody configuration on the drag of models tested in transonic wind tunnels. The model was a sting-supported axisymmetric body configuration. The model geometry was the same as used in a similar investigation conducted in the 1×1-m transonic wind tunnel of DFVLR in Göttingen, Germany. The current investigation was conducted in the AEDC 16-ft Transonic Wind Tunnel at Mach numbers from 0.6 to 1.4 and over a Reynolds number range of (8.12-21.7)×10⁶ based on model length. The results of this investigation, which show that forebody drag is not sensitive to changes in afterbody configuration, are in general agreement with previous results obtained at AEDC.

Nomenclature

A = local model cross-sectional area, ft²
A_{max} = maximum model cross-sectional area, 0.5185 ft²
$\bar{C}_D$ = drag coefficient obtained by integrating C_p from 0 to any X/L (i.e., drag buildup)
C_D = model pressure drag coefficient
C_{DAB} = afterbody pressure drag coefficient
C_{DFB} = forebody pressure drag coefficient
C_{PW1} = test section floor pressure coefficient for model with afterbody 1
C_{PW5} = test section floor pressure coefficient for model with afterbody 5
C_p = pressure coefficient, $=(P_l - P_\infty)/q_\infty$
L = model reference length, 5.417 ft
MS = model station aft of nose tip, in.
M_∞ = freestream Mach number
P_l = local surface static pressure, psfa
P_∞ = freestream static pressure, psfa
q_∞ = freestream dynamic pressure, psf
Re = Reynolds number based on model reference length and freestream conditions
X = axial distance measured from model nose, ft
θ = pressure orifice row location, deg

Introduction

A WIND-TUNNEL testing technique widely used to evaluate afterbody configuration effects on aircraft throttle dependent drag is based upon the assumption that drag variation caused by afterbody configuration changes are confined to the region of the model being changed. Typically, aircraft models are instrumented to measure only the forces on that portion of the fuselage which will be changed with variations in aircraft throttle position. Thus the validity of the assumption inherent in the testing technique is of critical importance to the correct assessment of total aircraft drag.

Results have been reported[1-3] which indicate that significant changes in forebody drag will occur when the afterbody configuration is changed. The model used in that investigation was axisymmetric and had interchangeable afterbodies. Data were obtained using the 1×1-m transonic wind tunnel of DFVLR in Göttingen, Germany. Based on those results, a project[4] was initiated at AEDC to perform an independent assessment of the validity of the testing technique. The model used for that assessment was axisymmetric with interchangeable afterbodies. The particular model used was selected because its area distribution was equivalent to the area distribution of an advanced fighter aircraft configuration. The testing was done in the AEDC 16-ft Transonic Wind Tunnel (16T). The results showed that large changes in afterbody drag can occur without causing any change in forebody drag.

Since the models tested in the AEDC and DFVLR wind tunnels had significantly different shapes, another project was initiated at AEDC to test the same model configuration used by Aulehla and Besigk in their investigation. A description of the experimental equipment and the test results of the AEDC project are presented.

Experimental Equipment

Model Configuration

An axisymmetric model with a contour specified by the equations given in Ref. 1 was fabricated for this investigation. Only afterbodies 1 and 5 were fabricated and tested since the effect of a maximum change in afterbody configuration was of interest. The model forebody and afterbody contours are described by third-order polynomials in X except for afterbody 5, which has a cylindrical section for $0.5 \le X/L \le 0.8125$. The model cross-sectional area distribution is shown in Fig. 1. Note that the intersection of the afterbody contour and the model support sting occurs at different X/L since the equations require the afterbody radius be zero at $X=L$. A schematic of the model and sting mounting is shown in Fig. 2, and a comparison of the model afterbodies is shown in Fig. 3. As shown, the afterbody configurations had very different contours. The model with afterbody 1 was 5.167 ft in length and with afterbody 5 was 5.323 ft in length. The model theoretical length, i.e., afterbody radius equal zero, was 5.417 ft and was the length used to calculate the model Reynolds number. The model maximum diameter was 0.8125 ft, which is 2.064 times larger than the model tested at DFVLR.

Model Sting and Installation

The dimensions of the model sting are shown in Fig. 4. The diameter of the section of the sting to which the model mounted was sized as close as was practical using the same

Presented as Paper 81-1443 at the AIAA/SAE/ASME 17th Joint Propulsion Conference, Colorado Springs, Colo., July 27-29, 1981; submitted Aug. 10, 1981; revision received Nov. 10, 1981. This paper is declared a work of the U.S. Government and therefore is in the public domain.

*Director, Project Analysis and Engineering, AEDC. Member AIAA.
†Project Engineer, 16T/S Projects Branch, Calspan/AEDC Division.

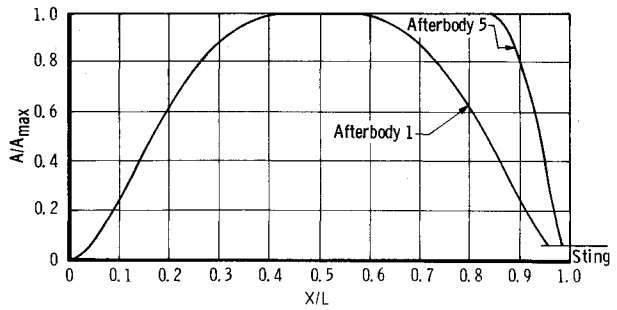

Fig. 1 Model cross-sectional area distributions.

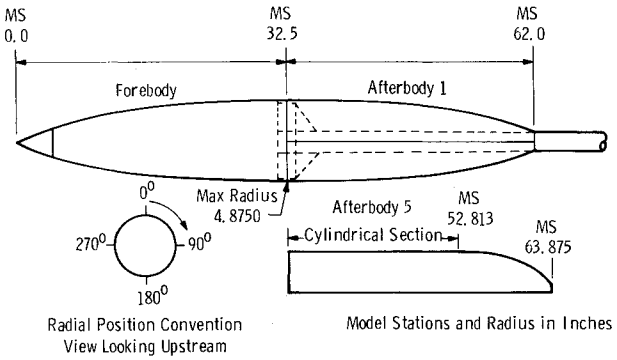

Fig. 2 Model and sting-mounting schematic.

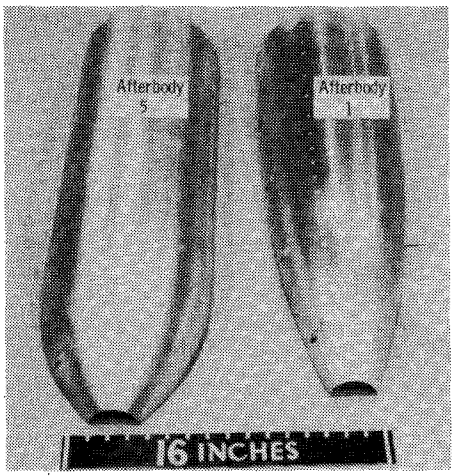

Fig. 3 Comparison of afterbody configurations.

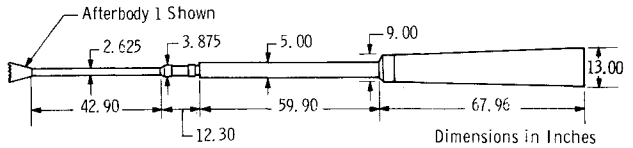

Fig. 4 AEDC sting configuration.

scale used to size the model. The overall sting configuration was determined using 1) the criteria recommended by Kennedy[5] to prevent interference from downstream sources and 2) the requirement that the model nose be located at station 6 in the wind-tunnel test section. The latter requirement was to locate the model in the same position used in the prior AEDC investigation.[4] The sting mounts into a support strut located in the aft region of the test section. The model installed in the AEDC tunnel (16T) is shown in Fig. 5.

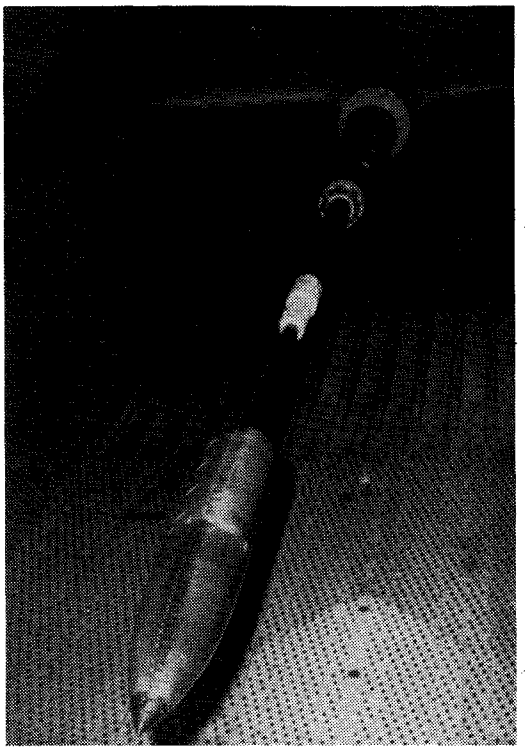

Fig. 5 Model installation in the AEDC Transonic Wind Tunnel (16T).

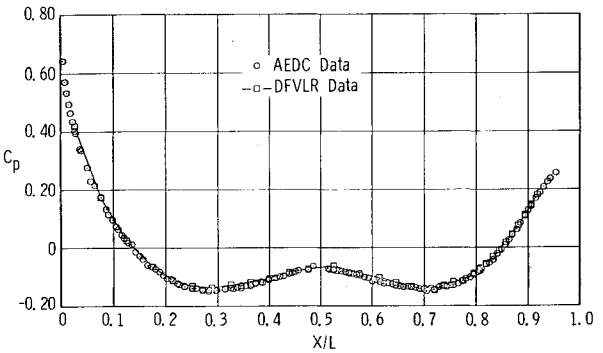

Fig. 6 Pressure distribution comparison for afterbody 1 at Mach number 0.8 and Reynolds number 15.708×10^6.

Instrumentation

Pressure orifices were installed on the model, the sting, and the test section floor centerline to obtain the data presented. The model and sting pressures were measured with 15-psid transducers and Scanivalves® mounted inside the model. The test section floor pressures were measured with the 16T differential pressure system.[6] All orifices were flush mounted, and special care was given to prevent damage to the orifice edges during model installation and testing.

The primary model data were obtained using pressure orifices located along the 90- and 270-deg rows of the model. A total of 142 and 140 orifices were used for the model with afterbody configurations 1 and 5, respectively. In addition, orifices were installed on the 180-deg row to duplicate the pressure orifice locations on the model tested at DFVLR. Two pressure orifices were installed on opposite sides of the sting at the location of the intersection of each afterbody and the sting. These were used to extend the pressure distributions to the trailing edge of the model. Twenty pressure orifices were installed at 1-ft intervals along the test section floor centerline. In addition, the 24 pressure orifices used in the DFVLR wind tunnel were duplicated.

Table 1 Test matrix

Mach no.	Reynolds no., $\times 10^{-6}$	Afterbody 1	Afterbody 5
0.60	8.125		X
	13.271	X	X
	21.667	X	X
0.80	10.020		X
	15.708	X	X
	21.667	X	X
0.85	21.667	X	X
0.90	10.563		X
	16.792	X	X
	21.667	X	X
0.95	21.667	X	X
1.10	21.667	X	X
1.20	21.667	X	X
1.40	20.583	X	X

Table 2 Data repeatability

Mach no.	Reynolds no., $\times 10^{-6}$	C_{DFB}	C_{DAB}	C_D
0.60	13.271	−0.0014	0.0089	0.0075
		−0.0027	0.0084	0.0057
0.80	15.708	−0.0008	0.0103	0.0095
		−0.0012	0.0101	0.0089
0.90	16.792	0.0007	0.0124	0.0131
		0.0006	0.0125	0.0131
0.95	21.667	0.0085	0.1352	0.1437
		0.0078	0.1379	0.1457

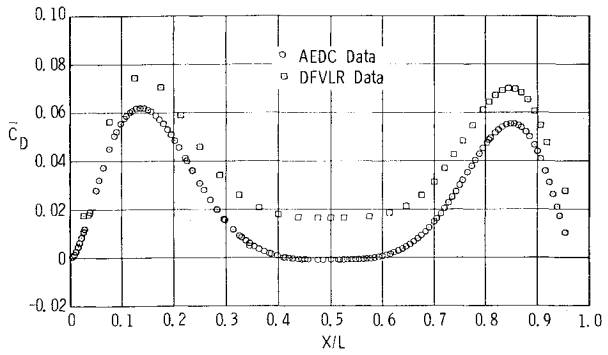

Fig. 7 Drag integration comparison for afterbody 1 at Mach number 0.8 and Reynolds number 15.708×10^6.

Test Matrix and Data Reduction

The test matrix shown in Table 1 was prepared so the range of parameters would be consistent with those used in the previous test at AEDC as well as match the conditions used in the tests at DFVLR. The model was fixed at 0-deg angle of attack for all test conditions. Data repeatability runs were made for four Mach numbers. The specific test conditions and data repeatability are shown in Table 2.

Pressure distribution data were reduced to coefficient form and integrated to obtain model drag coefficients. The integrations were performed using both the trapezoidal and a cubic spline fit integration method. The results were in excellent agreement since there were sufficient pressure orifices for the trapezoidal representation to be a very accurate approximation. The forebody drag coefficient, C_{DFB}, was obtained by integrating the pressure distribution, obtained using the 90- and 270-deg row pressure orifices, for $0 \le X/L \le 0.5$. The model stagnation pressure coefficient was calculated using the tunnel total pressure for subsonic Mach numbers and using the total pressure from the Rayleigh pitot formula for supersonic Mach numbers. The model drag coefficient, C_D, was obtained by integrating pressure distribution for $0 \le X/L \le 1.0$. The afterbody drag coefficient, C_{DAB}, was obtained as the difference between C_D and C_{DFB}. The drag coefficients were computed using the maximum model cross-sectional area, A_{max}, as the reference area.

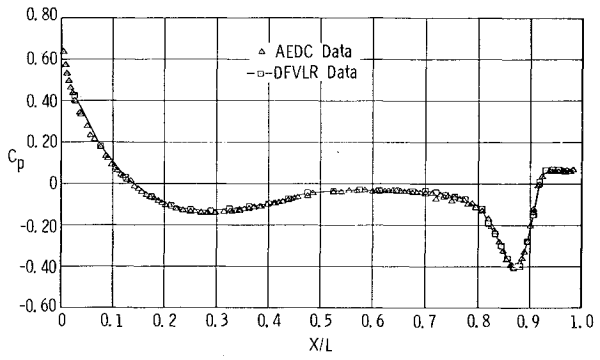

Fig. 8 Pressure distribution comparison for afterbody 5 at Mach number 0.8 and Reynolds number 15.708×10^6.

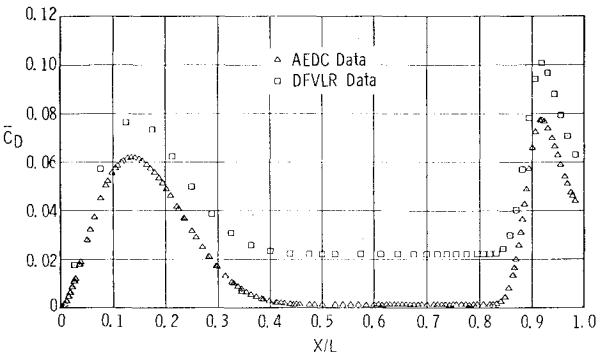

Fig. 9 Drag integration comparison for afterbody 5 at Mach number 0.8 and Reynolds number 15.708×10^6.

Results and Discussion

Data were obtained at Mach numbers and Reynolds numbers which would permit a direct comparison with data obtained in the DFVLR wind tunnel. Only the Mach number 0.8 comparisons are presented in this paper; however, these results are typical for the complete range of data obtained.

The model pressure distributions for afterbody 1 are shown in Fig. 6. The DFVLR data points are connected by straight lines which appear to indicate a slightly higher pressure distribution compared to the AEDC data. Although the difference between the two data sets in Fig. 6 is very small, a significant difference appears when the pressure data are integrated as shown in Fig. 7. The DFVLR data generate a higher drag on the forebody and appear as a nearly constant shift after $X/L = 0.3$. A major contributor to this difference in results could be the lack of adequate pressure orifices in the region $0 \le X/L \le 0.3$ of the model tested at DFVLR to obtain an accurate drag integration. The data comparisons for the model with afterbody 5 are shown in Figs. 8 and 9. These results are similar to the results for afterbody 1.

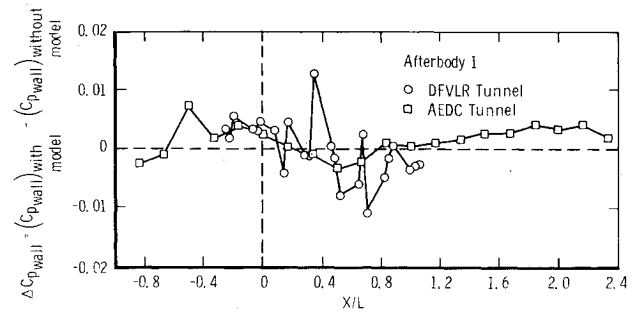

Fig. 10 Effect of model on tunnel wall pressure distribution at Mach number 0.8 and Reynolds number 15×10^6.

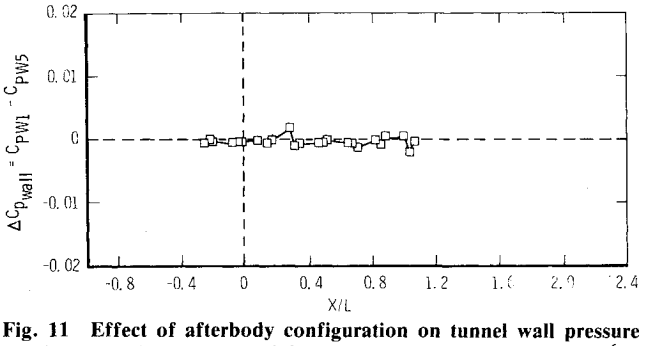

Fig. 11 Effect of afterbody configuration on tunnel wall pressure distribution at Mach number 0.8 and Reynolds number 15.708×10^6.

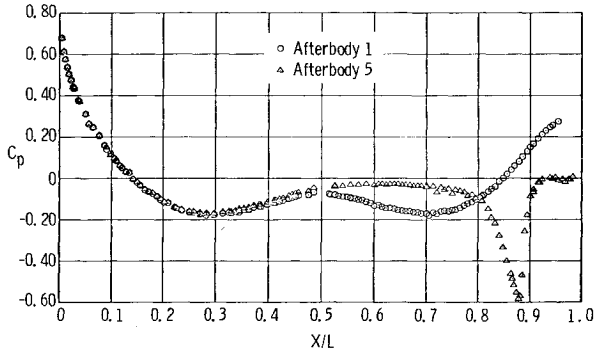

Fig. 12 Pressure distribution for Mach number 0.9 and Reynolds number 21.667×10^6.

It is well known that pressure drag integrations are very sensitive to small deviations in pressure distribution. For example, it would require only a 0.018 shift in the forebody pressure coefficients shown in Fig. 6 to generate the shift in the integrated drag coefficients shown in Fig. 7. Therefore one should always be concerned about the possibility of interference effects, such as model blockage, which could influence the model pressure distribution. A comparison of the AEDC and DFVLR wind-tunnel test section pressure distributions for the model with afterbody 1 and Mach number 0.8 is shown in Fig. 10. The set of pressure orifices installed in the AEDC tunnel which corresponds to the set installed in the DFVLR tunnel could not be used for this comparison since tunnel-empty data were not available. However, data from these pressure orifices are presented in Fig. 11 and document the influence of model configuration on the AEDC tunnel floor. The data from Figs. 10 and 11 indicate little effect of the model presence on the wind-tunnel floor pressures, especially in the AEDC tunnel. The model blockage in the AEDC and DFVLR wind tunnels was 0.203 and 1.131%, respectively. The test section wall was approximately 9.3 model diameters from the model in the AEDC tunnel and approximately 3.7 model diameters in the DFVLR tunnel.

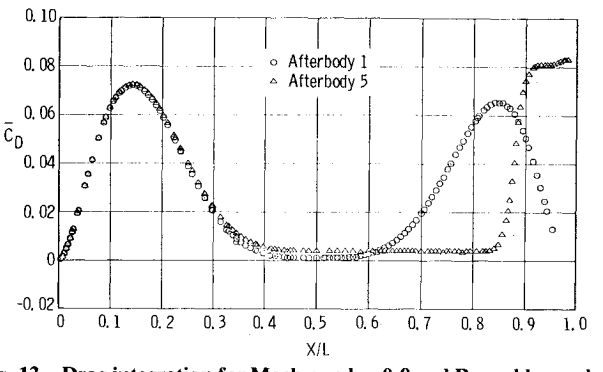

Fig. 13 Drag integration for Mach number 0.9 and Reynolds number 21.667×10^6.

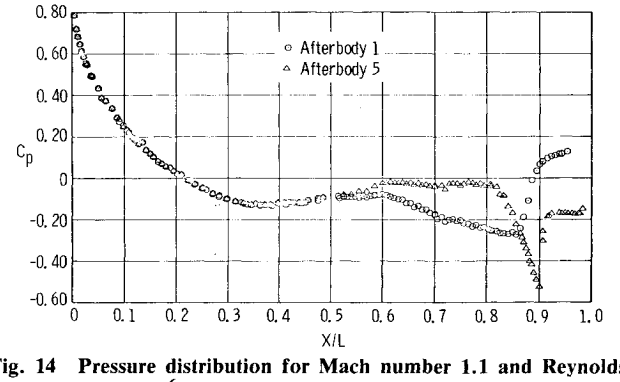

Fig. 14 Pressure distribution for Mach number 1.1 and Reynolds number 21.667×10^6.

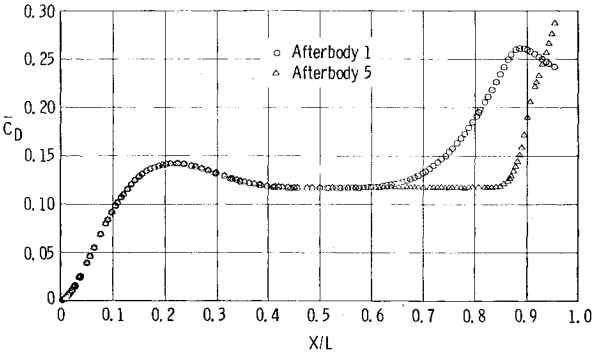

Fig. 15 Drag integration for Mach number 1.1 and Reynolds number 21.667×10^6.

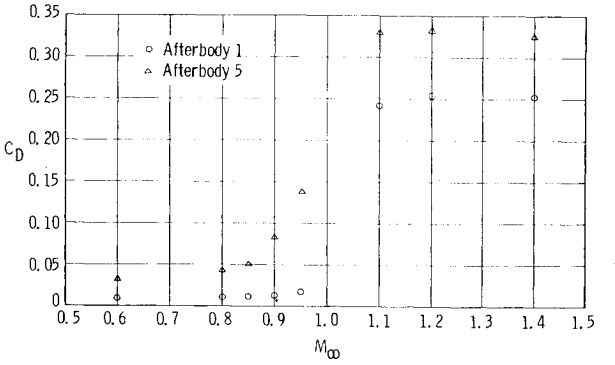

Fig. 16 Total drag variation with Mach number at Reynolds number 21.667×10^6.

In order to obtain the usual drag vs Mach number characteristics, which are of interest for an aircraft, each afterbody configuration was also tested with a constant Reynolds number over the Mach number range

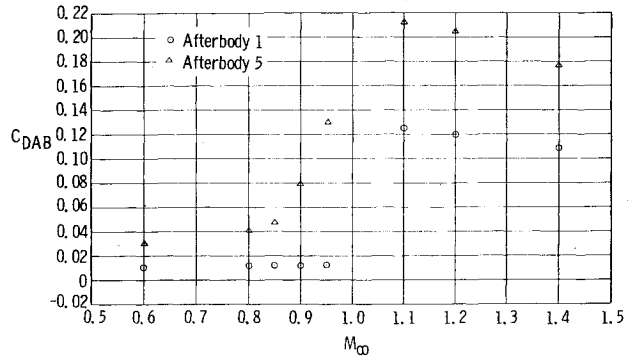

Fig. 17 Afterbody drag variation with Mach number at Reynolds number 21.667×10^6.

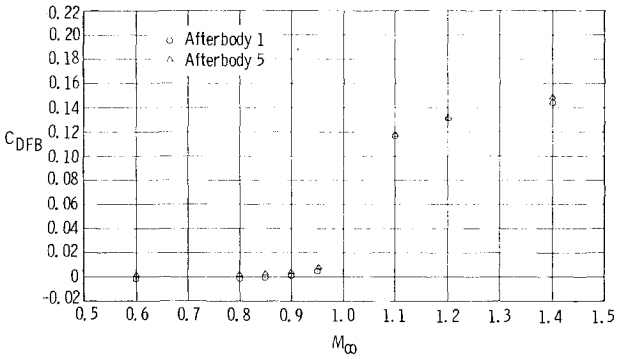

Fig. 18 Forebody drag variation with Mach number at Reynolds number 21.667×10^6.

$0.6 \leq M_\infty \leq 1.4$. The Reynolds number effects have been reported previously[4] and were not included as a part of this investigation. Typical results for the pressure distributions and drag integrations are shown in Figs. 12-15 for Mach numbers 0.9 and 1.1. As shown, significant changes occur in both afterbody pressure distributions and drag integrations with essentially no change in the corresponding data for the forebody. The total model drag coefficient, C_D, variation with Mach number is shown in Fig. 16, and as would be expected a significant variation was measured. The afterbody drag coefficient, C_{DAB}, is shown in Fig. 17. Again, a significant variation in the drag coefficient was measured. The forebody drag coefficient, C_{DFB}, is shown in Fig. 18 where it is shown that the forebody drag was insensitive to changes in afterbody configuration. This result is in agreement with that reported by Spratley et al.[4]

Conclusions

Two investigations have been conducted in the AEDC Transonic Wind Tunnel (16T) to assess the validity of a test technique currently used to obtain aircraft throttle dependent drag. One[4] used an axisymmetric model configuration having an area distribution equivalent to the area distribution of an advanced fighter type of aircraft. The other, reported herein, used the axisymmetric model configuration which had been used in the investigation by Aulehla and Besigk.[1-3] Although caution must be used in the selection of the metric portion of a wind-tunnel model, the results of the investigations at AEDC are in agreement and do not provide any basis for invalidating the testing technique currently used to obtain aircraft throttle dependent drag. It is important to emphasize the well-known requirement that adequate instrumentation and low-tunnel-blockage models must be used to accurately assess small but significant parameters when models are tested in transonic wind tunnels.

Acknowledgment

The research reported herein was conducted by the Arnold Engineering Development Center, Air Force Systems Command, Arnold Air Force Station, Tenn. Further reproduction is authorized to satisfy needs of the U.S. Government.

References

[1] Aulehla, F. and Besigk, G., "Reynolds Number Effects on Fore- and Aftbody Pressure Drag," AGARD-CP-150, 1975, Chap. 12.

[2] Aulehla, F. and Besigk, G., "Fore- and Aftbody Flow Field Interaction with Considerations of Reynolds Number Effects," AGARD-AG-208, 1975, Chapt. II-F.

[3] Aulehla, F., "Drag Measurement in Transonic Wind Tunnels," Paper 7 presented at the AGARD Specialists Meeting on Aircraft Performance Prediction Methods, Paris, France, Oct. 1977.

[4] Spratley, A.V., Thompson, E.R., and Kennedy, T.L., "Reynolds Number and Nozzle Afterbody Configuration Effects on Model Forebody and Afterbody Drag," AIAA Paper 77-103 , Jan. 1977.

[5] Kennedy, T.L., "An Evaluation of Wind Tunnel Test Techniques for Aircraft Nozzle Afterbody Testing at Transonic Mach Numbers," AEDC-TR-80-8 (AD-A091775), Nov. 1980.

[6] "Propulsion Wind Tunnel Facility," *Test Facilities Handbook*, 11th ed., Vol. 4, Arnold Engineering Development Center, April 1981.